On the Dual Effect of Mg Doping in $LiCoO_2$ and $Li_{1+\delta}CoO_2$: Structural, Electronic Properties, and ^7Li MAS NMR Studies

S. Levasseur, M. Ménétrier, and C. Delmas*

Institut de Chimie de la Matière Condensée de Bordeaux-CNRS and Ecole Nationale Supérieure de Chimie et Physique de Bordeaux, 87, Av. Dr A. Schweitzer, 33608 Pessac Cedex, France

Received January 14, 2002. Revised Manuscript Received May 22, 2002

HT-$Li_{x_0}Co_{1-y}Mg_yO_2$ (where x_0 is the Li/(Co + Mg) ratio; $x_0 = 0.98$, 1.0, 1.10; $y = 0.0$, 0.03, 0.06, and 0.10) materials were synthesized via a solid-state reaction. These samples were characterized by X-ray diffraction, ^7Li MAS NMR spectroscopy, and electrical properties measurements. The XRD study showed that pure phases are obtained for $0.0 \leq y < 0.10$ and $x_0 \geq 1.0$. ^7Li MAS NMR spectra of the Mg-doped phases exhibit two types of new signals at 55 ppm and 325, 7, −9, and − 27 ppm in addition to the signal at 0 ppm resulting from the presence of diamagnetic Co^{III} ions. On the basis of our general knowledge of Li NMR in layered oxides with electron spins, we suggest that Mg doping in $LiCoO_2$ always leads to the simultaneous presence of Co^{IV} ions (sharing an itinerant electron hole with neighboring Co^{III} ions) and, to a smaller extent, of intermediate spin $Co^{3+(IS)}$ ions trapped in a square-based pyramidal environment because of an oxygen vacancy. This feature is further enhanced by lithium overstoichiometry.

Introduction

$LiCoO_2$ is the most common positive electrode material for commercial Li-ion batteries because the compromise between its cost and cycling properties has not been equaled yet.[1,2] Its structure exhibits the layered α-$NaFeO_2$-type framework (space group $R\bar{3}m$) in which Co and Li planes alternate in the AB CA BC packing of oxygen layers.[3] In an attempt to extend the cycleability and enhance the capacity of the electrochemical Li//$LiCoO_2$ cells, numerous cations have been substituted for cobalt, among which one can mention the following ones: Ni,[4−7] Mn,[8,9] Cr,[10] Al,[11,12] or Fe.[13] In 1997, Tukamoto and West and Carewska et al. reported for the first time that substitution of Mg for Co could enhance the cycling properties of $LiCoO_2$ by strongly increasing the electronic conductivity of the starting material.[14,15] These authors reported an $LiCo_{1-y}Mg_yO_2$ solid solution domain for $0.0 \leq y \leq 0.08$ and hypothesized that the substitution corresponds to the $2Co^{III} \rightarrow 1Co^{IV} + 1Mg^{2+}$ scheme and, therefore, leads to the appearance of electron holes in the cobalt t_{2g} band. Besides, using ^7Li MAS NMR spectroscopy, we reported that synthesis of $LiCoO_2$ with a nominal Li/Co ratio strictly higher than 1 leads to the presence of NMR signals assigned to paramagnetic intermediate spin $Co^{3+(IS)}$ ions present in a square-based pyramidal environment because of the presence of O vacancies in the structure of the final material, with a $[Li]_{interslab}[Co_{1-\delta}Li_\delta]_{slab}[O_{2-\delta}]$ formula.[16] In the parent $Li(Ni,Mg)O_2$ system, Pouillerie et al. argued that Mg substitution could strongly improve the cycling properties by migration of the Mg^{2+} ions from the Ni layer to the interslab space after the first cycle at high potential, thus stabilizing the layered framework of the $LiNiO_2$ structure.[17,18] Very recently, Julien et al. reported an $LiCo_{0.50}Mg_{0.50}O_2$ material with a pure layered structure using sol−gel synthesis.[19]

From an applied point of view and to further investigate the question of the presence of paramagnetic species in $LiCoO_2$, we carried out a study of combined

(1) Mizushima, K.; Jones, P. C.; Wiseman, P. J.; Goodenough, J. B. *Mater. Res. Bull.* **1980**, *15*, 783.
(2) Abe, H.; Zaghib, K.; Tatsumi, K.; Higuchi, S. *J. Power Sources* **1995**, *54*, 236.
(3) Orman, H. J.; Wiseman, P. J. *Acta Crystallogr.* **1984**, *40*, 12.
(4) Delmas, C.; Saadoune, I.; Rougier, A. *J. Power Sources* **1993**, *43−44*, 595.
(5) Saadoune, I.; Delmas, C. *J. Mater. Chem.* **1996**, *6*, 193.
(6) Ueda, A.; Ohzuku, T. *J. Electrochem. Soc.* **1994**, *141*, 2010.
(7) Levasseur, S.; Ménétrier, M.; Delmas, C. *J. Electrochem. Soc.*, in press.
(8) Stoyanova, R.; Zhecheva, E.; Zarkova, L. *Solid State Ionics* **1994**, *73*, 233.
(9) Waki, S.; Dokko, K.; Itoh, T.; Nishizawa, M.; Abe, T.; Uchida, I. *J. Solid State Electrochem.* **2000**, *4*, 205.
(10) Jones, C. D. W.; Rossen, E.; Dahn, J. R. *Solid State Ionics* **1994**, *68*, 65.
(11) Jang, Y. I.; Huang, B.; Wang, H.; Maslkaly, G. R.; Ceder, G.; Sadoway, D. R.; Chiang, Y. M.; Liu, H.; Tamura, H. *J. Power Sources* **1999**, *81−82*, 589.
(12) Julien, C.; Nazri, G. A.; Rougier, A. *Solid State Ionics* **2000**, *135*, 121.
(13) Kobayachi, H.; Shigemura, H.; Tabuchi, M.; Sakaebe, H.; Ado, K.; Kageyama, H.; Hirano, A.; Kanno, R.; Wakita, M.; Morimoto, S.; Nasu, S. *J. Electrochem. Soc.* **2000**, *147*, 960.
(14) Tukamoto, H.; West, A. R. *J. Electrochem. Soc.* **1997**, *144*, 3164.
(15) Carewska, M.; Scaccia, S.; Arumugam, S.; Wang, Y.; Greenbaum, S. *Solid State Ionics* **1997**, *93*, 227.
(16) Levasseur, S.; Ménétrier, M.; Delmas, C. *Chem. Mater.*, submitted for publication.
(17) Pouillerie, C.; Croguennec, L.; Delmas, C. *Solid State Ionics* **2000**, *132*, 15.
(18) Pouillerie, C.; Perton, F.; Biensan, P.; Pérès, J. P.; Broussely, M.; Delmas, C. *J. Power Sources* **2001**, *96*, 293.
(19) Julien, C.; Camacho-Lopez, M. A.; Mohan, T.; Chitra, S.; Kalyani, P.; Gopukumar, S. *Solid State Ionics* **2000**, *135*, 241.

10.1021/cm021107j CCC: $22.00
Published on Web 07/25/2002

Mg doping and Li overstoichiometry. We synthesized $Li_{x_0}Co_{1-y}Mg_yO_2$ materials (where x_0 is the Li/(Co + Mg) ratio; $x_0 = 0.98$, 1.0, and 1.10; $y = 0.0$, 0.03, 0.06, and 0.10) and characterized them using X-ray diffraction (XRD), ^{7}Li MAS NMR spectroscopy, and electrical properties measurements.

Experimental Section

The starting $Li_{x_0}Co_{1-y}Mg_yO_2$ materials were prepared by direct solid-state reaction from Li_2CO_3 (Rhône Poulenc Rectapur %min. 99), Co_3O_4 (calcination at 450 °C for 12 h under O_2 of $Co(NO_3)_2$, $6H_2O$ Carlo Erba %min. 99) and MgC_2O_4, $2.09H_2O$ (Rhône Poulenc Rectapur %min. 99, hydratation rate determined by TGA). x_0 denotes the nominal Li/(Co + Mg) ratio of the mixture. The finely ground mixture was first heated at 600 °C for 12 h under O_2 and then heat-treated at 900 °C for 24 h under O_2 with intermediate grinding. To verify the thermal stability of the Mg-doped materials, a pure $LiCo_{0.94}Mg_{0.06}O_2$ phase was subsequently heat-treated at 900 °C for 5 days under oxygen. This material is called " annealed $LiCo_{0.94}Mg_{0.06}O_2$".

For the structure refinements, the XRD patterns were collected using a Siemens D5000 powder diffractometer with Cu Kα radiation and a graphite diffracted beam monochromator. The structures were refined using the Fullprof program with a pseudo-Voigt fitting function (Rietveld method).[20] To detect very low impurity levels (Co_3O_4, Li_2CO_3, MgO, etc.) in the background noise, XRD patterns were also systematically recorded using an INEL CPS120 in a Debye−Scherrer configuration with Co $K\alpha_1$ radiation, avoiding any fluorescence from cobalt atoms.

^{7}Li MAS NMR spectra were recorded on a Bruker MSL200 spectrometer at 77.7 MHz, with a standard 4-mm Bruker MAS probe. The samples were mixed with dry silica (typically 50% in weight) to facilitate the spinning and improve the field homogeneity because they may exhibit metallic or paramagnetic properties. The mixture was placed into a 4-mm-diameter zirconia rotor in a drybox. For all phases, a Hahn echo sequence $[t_{\pi/2}-\tau_1-t_\pi-\tau_2]$ was utilized to facilitate the phasing of all the signals and of their spinning sidebands and to ensure the observation of possibly very wide signals that would be lost during the receiver dead time in single-pulse experiments. The 90° pulse duration used ($t_{\pi/2}$) was equal to 3.05 μs. To synchronize the spin−echo with the first rotational echo, τ_1 was fixed to the rotor period $T_r = 1/\nu_r$, the spinning speed (ν_r) being 15 kHz. With such a Hahn echo sequence, phasing can be done easily with only zero-order correction if required and no baseline correction is needed. A 200-kHz spectral width was used, and the recycle time $D_0 = 1$ s is long enough to avoid T_1 saturation effects. The isotropic shifts reported in parts per million are relative to an external sample of 1 M LiCl solution in water.

Electronic conductivity measurements were carried out on sintered pellets (8 mm in diameter, 600 MPa pressure, and thermal treatment at 800 °C for 12 h under oxygen) with the four-probe direct current method in the 100−300 K range. Thermoelectronic power measurements were performed with homemade equipment.[21]

Because the purpose of this study is to emphasize the combined effect of Mg doping and Li overstoichiometry on the properties of $Li_{x_0}(Co,Mg)O_2$ phases, all the results reported were obtained for the same batch for each $Li_{x_0}Co_{1-y}Mg_yO_2$ material.

Results and Discussion

X-Ray Diffraction Study—Rietveld Refinements. All the $Li_{x0}Co_{1-y}Mg_yO_2$ materials crystallize in the trigonal system (space group $R\bar{3}m$) with a layered α-$NaFeO_2$-type structure. Pure phases were obtained for $y = 0.03$ and 0.06 and for Li/(Co + Mg) ratios $x_0 = 1.0$ and 1.10. The presence of MgO was observed for the $Li_{0.98}Co_{0.94}Mg_{0.06}O_2$, $LiCo_{0.90}Mg_{0.10}O_2$, and the " annealed $LiCo_{0.94}Mg_{0.06}O_2$ " materials. No trace of Li_2CO_3 or Co_3O_4 was detected in any sample. Moreover, in all cases, narrow diffraction lines were obtained, suggesting good crystallinity of the various materials.

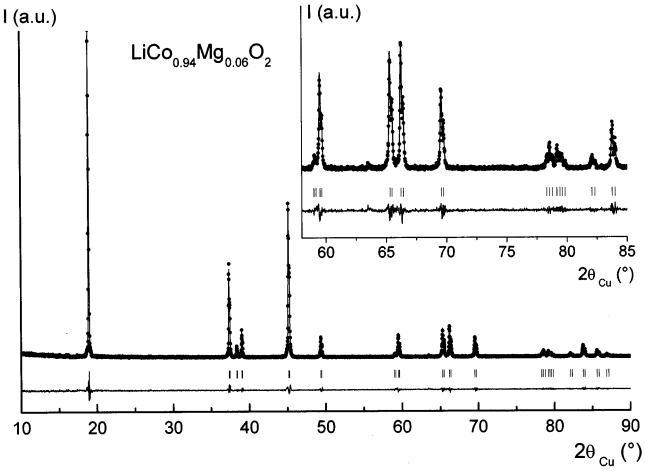

Figure 1. Observed and calculated XRD profiles for $LiCo_{0.94}Mg_{0.06}O_2$. Filled circles, observed; solid line, calculated; lower trace, difference plot; bars, position of the diffracted lines.

Table 1. Rietveld Refinement of the $LiCo_{0.94}Mg_{0.06}O_2$ X-ray Diffraction Spectrum (Site Occupancies Were Fixed)[a]

$Li_{1.0}Co_{0.94}Mg_{0.06}O_2$; space group $R\bar{3}m$; $a_{hex.} = 2.8212(1)$ Å; $c_{hex.} = 14.082(1)$ Å

		Wyckoff positions				
atom	site	x	y	z	occupancy	B (Å^2)
Li(1)	3b	0	0	1/2	1.0	0.60(60)
Mg(1)	3a	0	0	0	0.06	0.06(6)
Co(1)	3a	0	0	0	0.94	0.06(6)
O	6c	0	0	0.2601(4)	1.0	0.16(15)

[a] Profile function: pseudo-Voigt PV $= \eta L + (1 - \eta)G$; $\eta = \eta_0 + X(2\theta)$; $U = 0.038(6)$, $V = -0.004(4)$, $W = 0.004(1)$, $\eta_0 = 0.60(6)$, $X = 0.0006(10)$. Conventional Rietveld factors: $R_{wp} = 20.7$, $R_B = 2.99$, $\chi^2 = 1.81$, 14 refined parameters. The standard deviations were multiplied by the Scor parameter (Scorr = 2) to correct for local correlations.

All the $Li_{x_0}Co_{1-y}Mg_yO_2$ samples were characterized by Rietveld refinement of powder XRD data. Only the results for $LiCo_{0.94}Mg_{0.06}O_2$ are shown here (Figure 1) as all the patterns are similar to each other and to those reported elsewhere in the literature.[14,15,19] As the morphology of the crystallites could strongly influence the line intensity ratios in the diffraction patterns, all the samples for XRD were prepared in such a way that preferential orientation was minimized.[22] In a first step, the XRD pattern of the $LiCo_{0.94}Mg_{0.06}O_2$ phase was refined using a strictly two-dimensional (2D) model where global occupancies for the 3a (Co + Mg), 3b (Li), and 6c (O) sites were fixed to 1. The refinement results are shown in Table 1 and confirm the structural data reported elsewhere.[3,14] In all materials, the hypothesis of the presence of Co or Mg atoms in the crystallographic

(20) Rodriguez-Carjaval, J. *Fullprof, Laboratoire L. Brillouin (CEA-CNRS), http://www-llb.cea.fr/fullweb/powder.htm*.

(21) Dordor, P.; Marquestaut, E.; Villeneuve, G. *Rev. Phys. Appl.* **1980**, *15*, 1607.

(22) McCusker, L. B.; Von Dreele, R. B.; Cox, D. E.; Louer, D.; Scardi, P. *J. Appl. Crystallogr.* **1999**, *32*, 36.

Table 2. Hexagonal Cell Parameters and Oxygen *z* Position from Refinement of XRD Patterns for the Different $Li_{x_0}Co_{1-y}Mg_yO_2$ Materials

sample	$a_{hex.}$ (Å)	$c_{hex.}$ (Å)	*c*/*a*	$z_{ox.}$[a]
$LiCoO_2$[b]	2.8150(1)	14.0516(08)	4.99	0.2603(4)
$LiCo_{0.97}Mg_{0.03}O_2$	2.8178(1)	14.0723(10)	4.99	0.2602(6)
$Li_{1.10}Co_{0.97}Mg_{0.03}O_2$	2.8190(1)	14.0666(09)	4.99	0.2598(6)
$LiCo_{0.95}Mg_{0.05}O_2$	2.82002(9)	14.0735(6)	4.99	0.2594(6)
$LiCo_{0.94}Mg_{0.06}O_2$	2.8212(1)	14.0821(10)	4.99	0.2601(6)
$Li_{1.10}Co_{0.94}Mg_{0.06}O_2$	2.8220(1)	14.0814(10)	4.99	0.2600(6)
"$LiCo_{0.90}Mg_{0.10}O_2$"	2.8233(1)	14.0880(10)	4.99	0.2593(8)
"$Li_{0.98}Co_{0.94}Mg_{0.06}O_2$"	2.8184(2)	14.0735(10)	5.00	0.2602(6)
"$LiCo_{0.94}Mg_{0.06}O_2$" 900° C annealed	2.8165(1)	14.0625(10)	4.99	0.2602(4)

[a] 6c oxygen *z* position. [b] Reference 27.

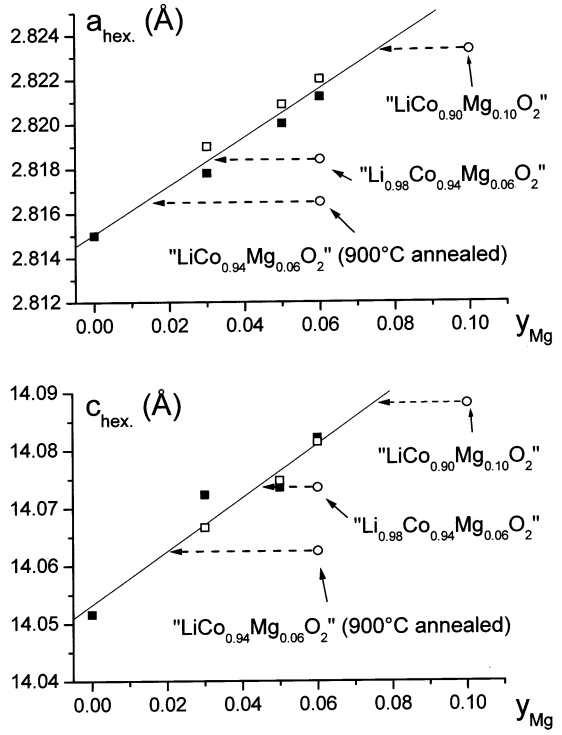

Figure 2. Evolution of the $a_{hex.}$ and $c_{hex.}$ hexagonal cell parameters as a function of *y* in the various $Li_{x_0}Co_{1-y}Mg_yO_2$ materials. Filled squares, $x_0 = 1$; open squares, $x_0 = 1.1$. The open circles correspond to samples whose actual *y* values differ from the nominal ones, as indicated by the horizontal dashed lines (see discussion in the text).

site of Li was rejected because the fit always leads to a negative or nil occupancy. Finally, because of the difficulty in quantifying Co absorption, no conclusion could be drawn about the presence of a small amount of Li or Mg ions in the cobalt site.

A general comparison of the structural data of the various $Li_{x_0}Co_{1-y}Mg_yO_2$ materials is given in Table 2 while the evolution of the refined hexagonal cell parameters is plotted as a function of the nominal Mg content, *y*, in Figure 2. One can observe a small increase of the $a_{hex.}$ and $c_{hex.}$ parameters with increasing *y* because of the larger size of Mg^{2+} compared to that of Co^{III} and Co^{IV} ions ($r_{Mg^{2+}} = 0.72$ Å, $r_{Co^{III}} = 0.545$ Å, $r_{Co^{IV}} = 0.53$ Å).[23] The *c*/*a* ratio remains constant whatever the Mg amount, suggesting the conservation of the strictly 2D character of the substituted materials, in good agreement with the high and constant value of the oxygen *z* position and the consequent difference in the slab (*S*) and interslab space (*I*) thicknesses ($S = 2.07$ Å and $I = 2.62$ Å for $LiCo_{1-y}Mg_yO_2$ whatever *y*; $S = 2.11$ Å and $I = 2.61$ Å for $Li_{0.98}Ni_{1.02}O_2$[24]).

Note on Figure 2 that the "$LiCo_{0.90}Mg_{0.10}O_2$" material, which contains some MgO, indeed exhibits parameters corresponding to lower Mg content; its actual Mg content therefore seems to be 7−8%. This observation is in complete agreement with the results by Tukamoto and West who found the solid solution limit in $LiCo_{1-y}Mg_yO_2$ for $y = 0.08$.[14]

The XRD pattern of the "$Li_{0.98}Co_{0.94}Mg_{0.06}O_2$" material shows traces of MgO, suggesting that the following reaction takes place during synthesis:

$$\text{"}Li_{0.98}Co_{0.94}Mg_{0.06}O_2\text{"} \rightarrow 0.98LiCo_{0.96}Mg_{0.04}O_2 + 0.02MgO$$

This reaction path, in which it is considered not possible to synthesize a Li-deficient Mg-doped phase, leads to the presence of an $LiCo_{1-y}Mg_yO_2$ phase with a real Mg content strictly lower than the nominal one; therefore, the refined cell parameters values corresponds to those of the material with a smaller Mg amount.

Finally, the XRD pattern of the "annealed $LiCo_{0.94}Mg_{0.06}O_2$" material shows the presence of a large amount of MgO, and the refined cell parameters of this material are close to those observed for undoped $LiCoO_2$, suggesting that the tendency to lose Li_2O at high temperature and the relative instability of Co^{IV} ions compared to Co^{III} lead to a quasi-complete phase separation:

$$LiCo_{0.94}Mg_{0.06}O_2 \rightarrow 0.03Li_2O + 0.94LiCoO_2 + 0.06MgO$$

Note that the absence of traces of Li_2O on the XRD pattern of the annealed "$LiCo_{0.94}Mg_{0.06}O_2$" material suggests that the Li_2O generated during the demixtion sublimates at temperatures around 900 °C, like for annealing of the $Li_{1.10}CoO_2$[16] and $LiNiO_2$[25] phases.

^{7}Li MAS NMR Study. *$Li_{x_0}Co_{1-y}Mg_yO_2$ Materials with $x_0 \leq 1.0$.* The ^{7}Li MAS NMR spectra of the various $Li_{x_0}Co_{1-y}Mg_yO_2$ ($x_0 \leq 1.0$) phases are shown in Figures 3 and 4. One can note on the spectra, in addition to the signal at 0 ppm due to the presence of Li^+ ions close to diamagnetic Co^{III} ions, the presence of a broad signal at 55 ppm and of weaker signals at 325 and −27 ppm, with a larger magnitude for materials with larger actual Mg contents.

Concerning the 55 ppm signal, referring to our previous work on deintercalated Li_xCoO_2 ($0.94 < x < 1.0$; $x_0 = 1.0$) phases, we know that the presence of localized electron spins on Co^{IV} ions within a diamagnetic Co^{III} lattice leads to a global loss of observability of the ^{7}Li MAS NMR signals because of a too strongly directly transferred hyperfine interaction between Li^+ and the neighboring Co^{IV} t_{2g} single electron.[26] In contrast, we have also shown that the presence of itinerant electron holes (resulting from Co^{IV} ions) leads in the Li_xCoO_2 (*x*

(23) Shannon, R. D.; Prewitt, C. T. *Acta Crystallogr.* **1969**, *B25*, 925.

(24) Rougier, A.; Gravereau, P.; Delmas, C. *J. Electrochem. Soc.* **1996**, *143*, 1168.

(25) Rougier, A. Thesis, University of Bordeaux I, France, 1995.

(26) Ménétrier, M.; Saadoune, I.; Levasseur, S.; Delmas, C. *J. Mater. Chem.* **1999**, *9*, 1135.

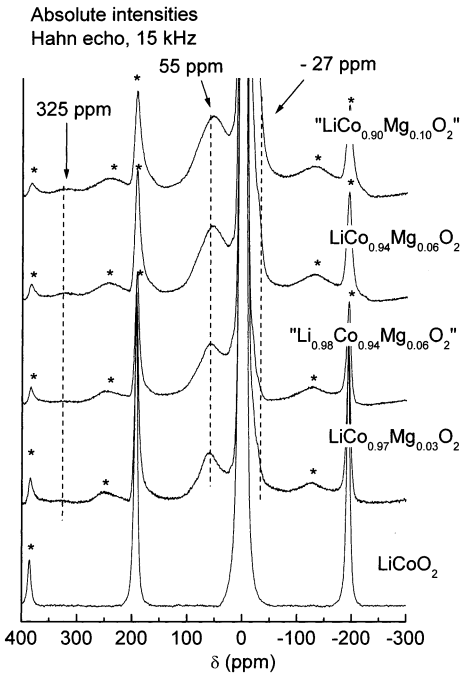

Figure 3. ^{7}Li MAS NMR spectra for the various $Li_{x_0}Co_{1-y}Mg_yO_2$ materials ($x_0 \leq 1.0$; $y = 0.0$, 0.03, 0.06, and 0.10) (77.7 MHz, spinning speed = 15 kHz, * = spinning sidebands).

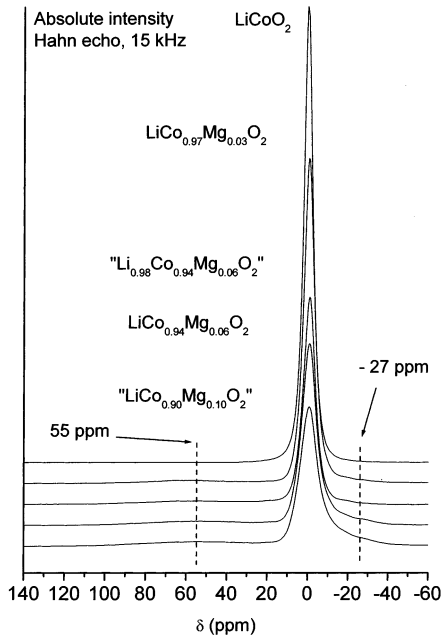

Figure 4. Expansion of the central signal of 15 kHz ^{7}Li MAS NMR spectra for the various $Li_{x_0}Co_{1-y}Mg_yO_2$ materials ($x_0 \leq 1.0$; $y = 0.0$, 0.03, 0.06, and 0.10).

≤ 0.94; $x_0 = 1.0$) materials to the presence of a new signal in the 50−120 ppm range, resulting from a Knight-shift-type interaction because of the participation of a lithium orbital at the Fermi level density of state.[26] Because of the echo sequence used for recording the NMR spectra, absolute intensities cannot be strictly compared for different samples because for example the Knight-shifted signal is less completely refocused by the echo due to a shorter T2 than the 0 ppm signal. However, on the basis of our previous investigations, we consider that the present ^{7}Li NMR spectra do not show significant loss of observation upon Mg substitution because the intensity is, to a large extent, transferred from the 0 ppm signal to the very broad additional signals at −27 and 55 ppm (and at 325 ppm, not shown in Figure 4). This, therefore, suggests that no localized electron spins such as those carried by Co^{4+} are present. Indeed, in the case of deintercalated Li_xCoO_2 ($0.94 < x < 1.0$; $x_0 = 1.0$) phases, where such Co^{4+} ions carrying localized electron spins are evidenced, we observed a decrease of the global intensity of the NMR spectra, the fwhm (full width at half-maximum) of the central signal remaining constant and no additional signal being observable in the frequency range studied, contrary to the observation in Figure 4.

Thus, we attribute the 55 ppm signal in the NMR spectra of the $Li_{x_0}Co_{1-y}Mg_yO_2$ ($x_0 \leq 1.0$) materials to a Knight-shift-type interaction, resulting from the presence of itinerant electron holes which induce metallic behavior in the sample, at least at the local scale.

As to the two signals at 325 and −27 ppm in Mg-doped samples, with larger magnitudes for materials with larger magnesium contents, their origin will be discussed in detail in the next section.

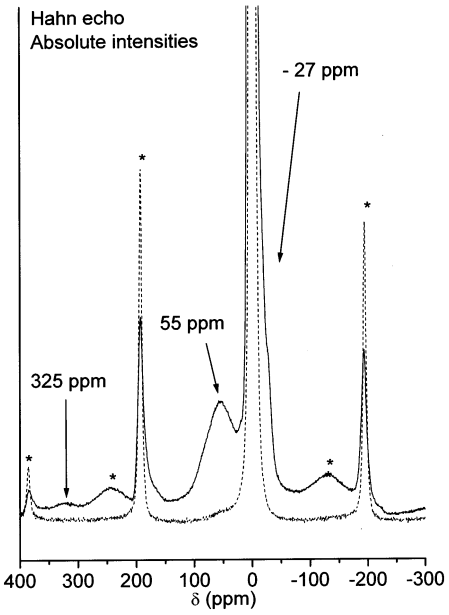

Figure 5. ^{7}Li MAS NMR spectra for the $LiCo_{0.94}Mg_{0.06}O_2$ material before (solid line) and after (dashed line) long heat treatment (77.7 MHz, spinning speed = 15 kHz, * = spinning sidebands).

Figure 5 shows the ^{7}Li MAS NMR spectra of the $LiCo_{0.94}Mg_{0.06}O_2$ material before and after annealing at 900 °C (5 days under O_2). The spectrum of the latter material is close to that of undoped $LiCoO_2$ ($x_0 = 1.0$) and does not show anymore the features related to the presence of Mg in the structure (i.e., 325, 55, and −27 ppm signals), in very good agreement with our XRD conclusions.

$Li_{x_0}Co_{1-y}Mg_yO_2$ Materials with $x_0 > 1.0$. Figures 6 and 7 show the comparison of the ^{7}Li MAS NMR spectra of the 3% and 6% Mg-doped phases synthesized without and with 10% Li excess. The signal at 55 ppm is partially reduced and less well-defined in the $Li_{1.10}Co_{1-y}Mg_yO_2$ ($y = 0.03$ and 0.06) phases than in the ones synthesized without any lithium excess. This partial disappearance of the " Knight-shift " interaction is quite similar to that observed at the beginning of deintercalation in the Li_xCoO_2 ($x_0 > 1.0$) system, where because

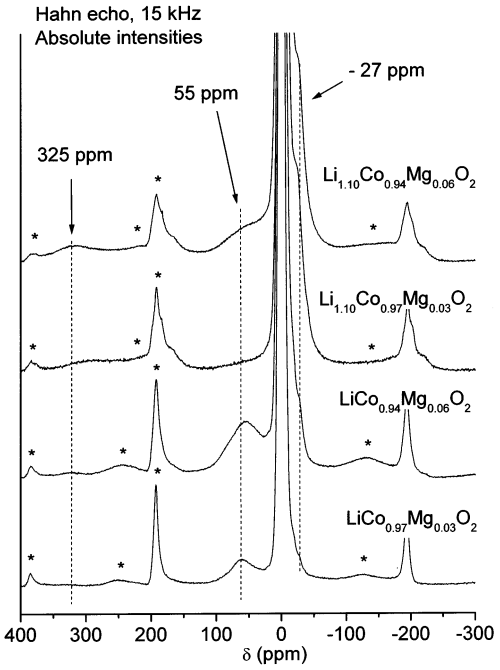

Figure 6. ^{7}Li MAS NMR spectra for the various $Li_{x_0}Co_{1-y}Mg_yO_2$ materials ($x_0 \geq 1.0$; $y = 0.03$ and 0.06) (77.7 MHz, spinning speed = 15 kHz, * = spinning sidebands).

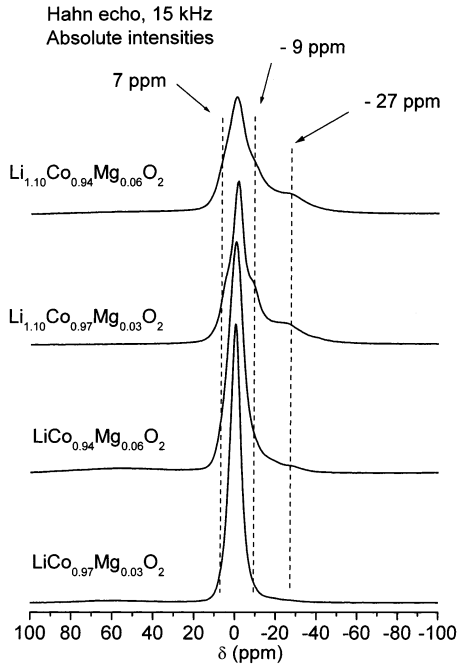

Figure 7. Expansion of the central signal of 15-kHz ^{7}Li MAS NMR spectra for the various $Li_{x_0}Co_{1-y}Mg_yO_2$ materials ($x_0 \geq 1.0$; $y = 0.03$ and 0.06).

of the presence of structural defects, the delocalization upon deintercalation only takes place in very small zones of the crystal.[27]

Furthermore, one can see, on the $Li_{1.10}Co_{1-y}Mg_yO_2$ ($y = 0.03$ and 0.06) NMR spectra, the signals at 325 and −27 ppm, which have already been observed for Mg-doped phases with $x_0 = 1.0$. In addition, note that two shoulders on the central line become clearly visible at 7 and −9 ppm (Figure 7). This set of signals at 325, 7, −9, and −27 ppm is very similar to the one observed in the case of undoped $Li_{x_0}CoO_2$ ($x_0 > 1.0$) phases. In this latter system, three signals at 185, −16, and −40 ppm are observable in addition to two shoulders on the central signal at 3 and −6 ppm, the origin of which was assigned to the presence of Li^+ ions close to a structural defect related to paramagnetic Co^{3+} ions in an intermediate spin state (labeled $Co^{3+(IS)}$) and to oxygen vacancies. The 185 ppm signal was considered to arise from Li^+ ions with one $Co^{3+(IS)}$ ion as the first neighbor (90° interaction via the overlap with the O orbital), the signals at −16 and −40 ppm being attributed to Li^+ ions with respectively one and two $Co^{3+(IS)}$ ions as second neighbors (180° interaction via oxygen); the shoulders at 3 and −6 ppm are due to Li^+ ions in the vicinity of the oxygen vacancy, which generates various mechanisms for the transfer of the hyperfine interaction.[16]

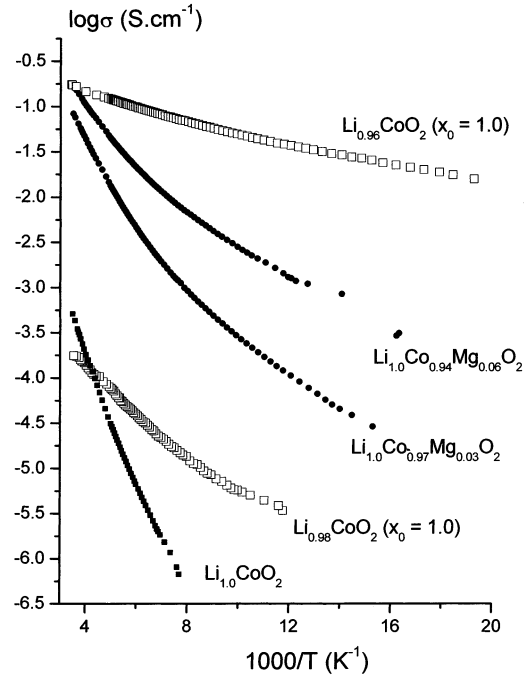

Figure 8. Variation of the logarithm of the electrical conductivity vs reciprocal temperature in the $LiCo_{1-y}Mg_yO_2$ ($y = 0.0$, 0.03, and 0.06) phases. Results for Li_xCoO_2 ($x = 0.98$, 0.96; $x_0 = 1.0$) deintercalated phases are also plotted.[26]

The similarity of the NMR spectra for $Li_{x_0}CoO_2$ ($x_0 > 1.0$) and $Li_{x_0}Co_{1-y}Mg_yO_2$ phases let us think that a structural defect leading to the presence of both $Co^{3+(IS)}$ ions and oxygen vacancies is also present in the Mg-doped materials; we attribute the signal at 325 ppm to lithium ions with one $Co^{3+(IS)}$ as the first neighbor, the signal at −27 ppm being due to Li^+ ions with $Co^{3+(IS)}$ as the second neighbor, and the shoulders at 7 and −9 ppm being related to lithium ions close to the oxygen defect. Note that these shoulders also exist in the $Li_{x_0}Co_{1-y}Mg_yO_2$ ($x_0 = 1.0$) NMR spectrum but their relative intensity is very much lower than in the case of the Mg-doped phases synthesized with $x_0 > 1.0$ (Figure 7). The difference observed in the chemical shift values for the $Li_{x_0}CoO_2$ ($x_0 > 1.0$) and $Li_{x_0}Co_{1-y}Mg_yO_2$ phases is probably due to differences in the local distortions (imposed by Mg or Li substitution) in the two systems.

Electrical Properties Study. *Electronic Conductivity Measurements.* Figure 8 shows the variation of the

(27) Levasseur, S.; Menetrier, M.; Suard, E.; Delmas, C. *Solid State Ionics* **2000**, *128*, 11.

Table 3. Electronic Conductivity Activation Energy vs y in the $LiCo_{1-y}Mg_yO_2$ (y = 0.0, 0.03, and 0.06) Phases in the 190−290 K Temperature Range[a]

	$Li_{1.0}CoO_2$	$Li_{0.98}CoO_2$ ($x_0 = 1.0$)	$Li_{0.96}CoO_2$ ($x_0 = 1.0$)	$LiCo_{0.97}Mg_{0.03}O_2$	$LiCo_{0.94}Mg_{0.06}O_2$
ΔE_a (eV) (190−290 K range)	0.16	0.05	0.02	0.11	0.07

[a] Activation energy of Li_xCoO_2 (x = 0.98, 0.96; x_0 = 1.0) deintercalated phases is also reported.[26]

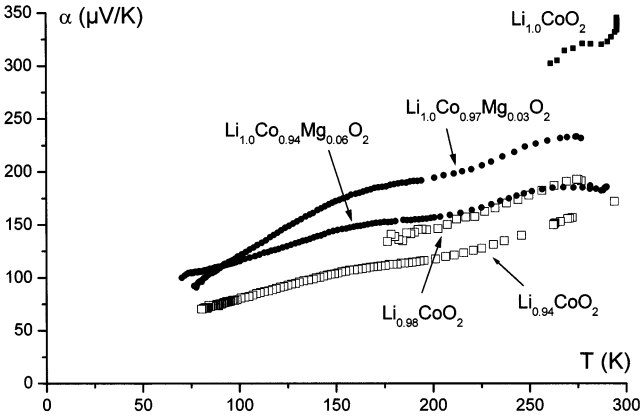

Figure 9. Thermal variation of the Seebeck coefficient in the $LiCo_{1-y}Mg_yO_2$ (y = 0.0, 0.03, and 0.06) phases. Results for Li_xCoO_2 (x = 0.98, 0.94; x_0 = 1.0) deintercalated phases are also plotted.[26]

electronic conductivity versus reciprocal temperature for the $LiCo_{1-y}Mg_yO_2$ (y = 0.0, 0.03, and 0.06) phases. For comparison, the curves of the semiconducting electrochemically deintercalated Li_xCoO_2 (x = 0.98, 0.96; x_0 = 1.0) phases are also plotted.[26]

As evidenced by previous studies, one can note the increase of the direct current (dc) conductivity with increasing Mg content in the structure.[14,15] However, in all cases, a global semiconducting behavior is evidenced as the dc conductivity remains thermally activated whatever the Mg amount. Nevertheless, the activation energy decreases in the $LiCo_{1-y}Mg_yO_2$ phases with increasing y (Table 3).

Note that the activation energy measured by dc conductivity remains quite high for the Mg-doped samples compared to that of the deintercalated $Li_{0.98}CoO_2$ and $Li_{0.96}CoO_2$ phases which contain 2 and 4% of Co^{IV} ions, respectively. This point will be discussed in the following section.

Thermoelectronic Power Measurements. Figure 9 shows the thermopower data in the 75−300 K range for the $LiCo_{1-y}Mg_yO_2$ (y = 0.0, 0.03, and 0.06) phases. In all cases, the positive value of the Seebeck coefficient shows that holes are the main charge carriers. Indeed, as Mg^{2+} enters the structure substituting for trivalent cobalt, Co^{IV} ions with one hole in the t_{2g} orbital ($t_{2g}5$) are created to ensure the charge compensation.[14,15]

The large values of the thermopower for all the Mg-doped phases are typical of a global semiconducting behavior and in good agreement with the dc conductivity results. The decrease in the values of the Seebeck coefficient with increasing Mg content reflects the increase in the concentration of the charge carriers in the materials.

General Discussion

The present study confirms all the previous results by Tukamoto and West and Carewska et al., proving the layered character of the $LiCo_{1-y}Mg_yO_2$ phases, thus showing that the Mg^{2+} ions substitute for Co, leading to the appearance of (formally) Co^{IV} ions.[14,15] Whereas ^{7}Li NMR shows a Knight-shift-type signal, the electric properties do not show evidence of metallic character. In fact, one has to take into account electrical neutrality around the substituting Mg^{2+} ions so that electron delocalization can only occur between the Co ions surrounding an Mg^{2+} ion. This induces metallic behavior at the local scale, but these domains do not percolate, leading to an increase in the dc conductivity vs $LiCoO_2$, but to overall nonmetallic properties. The absolute value of the dc conductivity increases and the activation energy decreases with increasing y in $LiCo_{1-y}Mg_yO_2$ because the number and proximity of "metallic domains" increase in the structure. However, it appears that the existence of such small "metallic zones" located around magnesium in the case of the $LiCo_{1-y}Mg_yO_2$ phases, and separated by poorly conducting zones, leads to a smaller conductivity than that generated by the Co^{III}/Co^{IV} hopping mechanism created upon lithium deintercalation from stoichiometric $LiCoO_2$, which occurs throughout the whole material and which can be associated, in the interslab space, with Li/vacancy mobility.

In the $LiCo_{1-y}Mg_yO_2$ materials, it is remarkable that the few Co^{IV} ions due to Mg substitution produce delocalized (i.e., itinerant) electrons, contrary to those created in Li_xCoO_2 at the beginning of the deintercalation.[26] This suggests that the local Co−Co distances are perturbed by the presence of Mg^{2+}. Furthermore, the number of cobalt ions involved in a possible electron delocalization is higher in the $LiCo_{1-y}Mg_yO_2$ phases (six cobalt ions around one Mg^{2+}) than in the Li_xCoO_2 system (only three cobalt ions in a given layer around one Li^+ vacancy), which may lead to a stronger tendency to create a conduction band in the Mg-doped phases.

However, our ^{7}Li MAS NMR spectroscopy and XRD study shows that it is not possible to synthesize $LiCo_{1-y}Mg_yO_2$ phases where Mg ions, while replacing Co, would lead only to the appearance of Co^{IV} ions, leading to the $[Li]_{interslab}[Co^{IV}_yMg^{2+}_yCo^{III}_{1-2y}]_{slab}O_2$ chemical formula. Indeed, substitution of Mg for Co always leads to weak extra NMR signals, similar (although with different isotropic shifts) to those observed in the case of Li-overstoichiometric $Li_{x_0}CoO_2$ phases ($x_0 > 1.0$).[16] A tendency of both generating Co^{IV} ions and another type of paramagnetic Co species which induces NMR results comparable to those obtained in the case of $Li_{x_0}CoO_2$ ($x_0 > 1.0$) phases was already observed by Carewska et al.[15] It is important to note that these extra NMR signals are present for the Mg-substituted samples whatever the Li stoichiometry. Indeed, a nominal composition of $Li_{0.98}(Co,Mg)O_2$ leads to a material containing less Mg, but exhibiting the extra signals. For Li-overstoichiometric compositions, the same signals are again observed, with a much stronger intensity. In the case of the Li-overstoichiometric $Li_{x_0}CoO_2$ phases ($x_0 > 1.0$), we

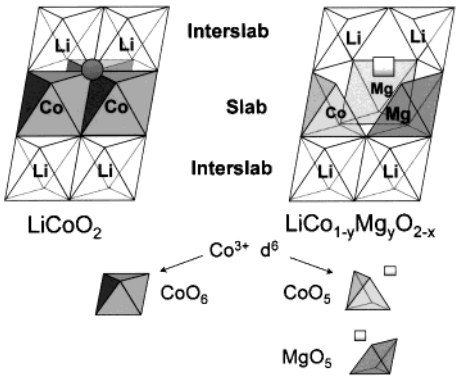

Figure 10. Schematic representation of the local environment for Mg and Co ions in the vicinity of an oxygen vacancy evidenced in the $Li_{x_0}Co_{1-y}Mg_yO_2$ materials.

attributed the extra NMR signals to the presence of $Co^{3+(IS)}$ ions, associated with a Li/Co ratio higher than 1, and implying a chemical formula $[Li]_{interslab}[Co^{III}{}_{1-3\delta}Co^{3+(IS)}{}_{2\delta}Li^{+}{}_{\delta}]_{slab}[O_{2-\delta}]$.[16] In the case of the Mg-doped $Li_{x_0}Co_{1-y}Mg_yO_2$ ($x_0 = 1.0$) phases, one can imagine a model where Mg^{2+} ions in substitution for Co^{III} would act as extra Li^+ ions in $Li_{1+x}CoO_2$, concerning the formation of oxygen vacancies for charge compensation. If two MgO_6 octahedra share an edge, the charge compensation at the local scale would not lead to the creation of two adjacent Co^{IV} ions (sharing an itinerant electron hole with neighboring Co^{III} ions) but to the creation of an oxygen vacancy spatially associated to these two Mg^{2+} ions, which would therefore be in an MgO_5 square-based pyramidal environment. As can be observed in Figure 10, this peculiar environment tends to stabilize a $Co^{3+(IS)}$ ion in the square-base pyramid, which shares a corner (O vacancy) with the two MgO_5 pyramids. The distortion of the local geometry imposed by these MgO_5 pyramids leads to Li−O and Co−O distances different from those observed in the $Li_{1+x}CoO_2$ system and therefore to different values for the isotropic NMR shifts.[16] This hypothetical model leads to a chemical formula close to $[Li]_{interslab}[Co^{III}{}_{1-t-\delta-y}Co^{IV}{}_t\ Co^{3+(IS)}{}_{\delta}Mg^{2+}{}_y]_{slab}[O_{2-\delta}]$. When excess lithium is also added in Mg-substituted materials, the same mechanism as in the case of the $Li_{1+x}CoO_2$ phase seems to occur. However, the fact that the Fermi contact shifts observed for the NMR signals are the same as those in the Li-stoichiometric $LiCo_{1-y}Mg_yO_2$ phase and different from those in the $Li_{1+x}CoO_2$ system suggests that the oxygen vacancies (and therefore the resulting $Co^{3+(IS)}$ ions) related to charge compensation for Mg^{2+} and for Li^+ are located in the same defect. This is also confirmed by the fact that annealing of an $LiCo_{0.94}Mg_{0.06}O_2$ phase leads to the disappearance of both the $Co^{3+(IS)}$ and the Mg^{2+} ions. Note also that the electronic delocalization induced by the Co^{IV} ions around Mg, and associated with the 55 ppm signal on the ^7Li MAS NMR spectra, is strongly perturbed in Li-overstoichiometric $Li_{1.10}Co_{1-y}Mg_yO_2$ phases where more $Co^{3+(IS)}$ ions (and structural defects) are evidenced than in the Li-stoichiometric case.

It therefore appears that Mg substitution leads to two different mechanisms for the charge compensation, namely, creation of (formally) Co^{IV} ions and also, to a smaller extent, of oxygen vacancies, which lead to a structural defect stabilizing $Co^{3+(IS)}$ ions. This seems to mean that the synthesis conditions are not oxidizing enough to generate numerous Co^{IV} ions. However, the latter mechanism, which necessarily implies two Mg ions next to each other for Li-stoichiometric samples, is favored in the presence of an excess of lithium (which by itself would lead to oxygen vacancies) at the expense of the Co^{4+}-type charge compensation mechanism. Nevertheless, the exact nature of the defect, implying both Mg and Li substitution for Co around an oxygen vacancy, remains unknown.

The combined effects of Mg substitution and Li-overstoichoimetry on the deintercalation mechanisms will be reported elsewhere.[28]

Acknowledgment. The authors wish to thank A. Audemer, L. Gautier, and J. Scoyer for fruitful discussions, E. Marquestaut and R. Decourt for technical assistance with the electrical properties measurements, J. Hirshinger and B. Meurer for the use of their NMR spectrometer, and Umicore, ANRT, and Région Aquitaine for financial support.

CM021107J

(28) Levasseur, S.; Ménétrier, M.; Delmas, C. *J. Power Sources*, submitted for publication.